The Linear and Nonlinear Bending Analyses of Functionally Graded Carbon Nanotube-Reinforced Composite Plates Based on the Novel Four-Node Quadrilateral Element

Hoang Lan Ton-That

Faculty of Civil Engineering, Ho Chi Minh City University of Architecture, 196 Pasteur Street, District 3, Ho Chi Minh City, Viet Nam
E-mail: lan.tonthathoang@uah.edu.vn

Received 07 September 2020; Accepted 19 October 2020;
Publication 27 November 2020

Abstract

This paper presents the linear and nonlinear analyses of functionally graded carbon nanotube- reinforced composite (FG-CNTRC) plates using a four-node quadrilateral element based on the C^0-type of Shi's third-order shear deformation theory (C^0-STSDT). Shi's theory is taking the advantages and desirable properties of the third-order shear deformation theory. Besides, material properties of FG-CNTRC plates are changed from the bottom to top surface and based on the rule of mixture. Numerical results and comparison with other reference solutions suggest that the advantages of the present element are accuracy and efficiency in analysis of FG-CNTRC plates. Some nonlinear numerical results of FG-CNTRC plates are also given in this paper and this contributes to providing additional data for future research work.

Keywords: Linear and nonlinear bending, Shi theory, C^0 type, four-node quadrilateral element.

European Journal of Computational Mechanics, Vol. 29_1, 139–172.
doi: 10.13052/ejcm2642-2085.2915
© 2020 River Publishers

1 Introduction

In the references [1, 2], we can see that carbon nanotubes (CNTs) with their outstanding features have made a big step forward for materials science. Carbon nanotubes (CNTs) have attracted great attention for their remarkable electrical, thermal and mechanical properties [3–6]. From the structural review, their material properties are listed as high strength, low density, stiffness, and so on. And they become a good candidate for composite structures. For this reason, linear and nonlinear behaviors of FG-CNTRC plates need to be studied particularly.

Besides developing and manufacturing novel advanced engineering materials, many theories have been introduced into linear and nonlinear analyses from thin to thick plates such as the classical plate theory (CPT), the first-order shear deformation theory (FSDT), the higher-order shear deformation theory (HSDT), the layer-wise theory (LWT) and variable kinematics models. The first-order shear deformation theory (FSDT) is commonly used because of its low computational cost and simplicity [7–9]. But we may easily recognize that the third-order shear deformation plate theories are the accurate theories and effective due to the quadratic variation of the transverse shear strains and stresses along the thickness of plate as well as the shear locking free. In the other hand, numerical methods have been expanded for the analysis of composite plate structures as given by Yang et al. [9], Leissa [10], Aydogu [11], Liew et al. [12, 13], Lee et al. [14], Nguyen-Xuan et al. [15–17], Ton-That et al. [18–23], etc. Specifically, we can mention a survey of recent finite elements by Yang et al. [9] which includes the degenerated approach [24-26], stress-resultant-based formulations [27, 28] and Cosserat surface approach [29], reduced integration with stabilization [30–32], incompatible modes approach [33, 34], enhanced strain formulations [35–37], 3-D elasticity elements [38, 39], drilling degree of freedom elements [18, 40–42], co-rotational approach [43, 44] and higher-order theories for composites [45, 46]. Besides the standard finite element methods, the smoothed finite element formulation for static, free vibration and buckling analyses of composite plates was based on a combination of node-based smoothing discrete shear gap method with the higher-order shear deformation plate theory [16]. The formulation had used only linear approximations and its implementation into finite element programs was quite simple and efficient. With an alternative alpha finite element method under discrete shear gap technique, Nguyen-Xuan et al. [17] presented a new approach for analysis of composite plates. The improved four-node element for analysis of composite plate structures

based on twice interpolation strategy was given by Ton-That et al. [20, 21]. Many desirable characteristics of these efficient numerical methods were shown as continuous nodal gradients, higher-order polynomial basis, no increase in number of the degree of freedom of the system and so on.

Going back to FSDT with clear mentions, finite element formulation only requires C^0 continuous shape functions as well as the weak-form equations only require the first derivative of displacement field. However, shear locking phenomenon occurs when the thickness-to-length ratio of plate gradually approaches zero and it can be handled using reduced integration. The series of the sort of elements based on mixed interpolation of tensorial components [14], twice interpolation strategy [20, 21], discrete shear gap [16], etc. have been developed to overcome shear locking, respectively.

With the higher-order shear deformation theory (HSDT), we recognize that it is widely used because it does not need shear correction factors and gives accurate transverse shear stresses. But with low-order finite elements such as four-node quadrilateral element, the need of C^1-continuous approximation for the displacement fields in the higher-order shear deformation theory causes some impediments. To overcome these shortcomings, the HSDT is revised form in which only requires C^0 continuity for displacement fields (C^0-HSDT). In the C^0-HSDT, two additional variables are joined, and thence the first derivative of transverse displacements is only required. Besides, Shi [19, 47] recently gave a simple third-order shear deformation theory that was applied to static analysis of isotropic and orthotropic structures. The solutions achieved by this theory have shown to be highly accurate and more reliable than others. From these reasons, a novel four-node quadrilateral element with seven degrees-of-freedom per node related to C^0-type of Shi's third-order shear deformation theory (C^0-STSDT), is firstly introduced for linear and nonlinear analyses of the FG-CNTRC plates. Based on the idea of using the high-order shear deformation theory through the C^0-type, the achieved results are given completely reliable without any regrettable phenomena.

On the other hand, the paper of Yengejeh et al. [48] was given to highlight and categorize the most important and novel studies conducted to explore the mechanical behavior of nano-composites reinforced with carbon nanotubes (CNTs). The existing papers cover the mechanical performance of reinforced composites, both theoretically and experimentally, which allows an accurate estimate of the mechanical performance of these nano-structures. It was addressed that the predictive methods can be categorized as models based on unit cells with a single fiber, models considering a unit cell with a larger

number of fibers, and how the fibers are modeled: as a 1D, 2D, or 3D configuration. Furthermore, they reviewed two different experimental methods (destructive and non-destructive) in order to highlight more knowledge in this field of research. Fisher et al. [49] established a model joining micro mechanical approaches and finite element outputs to predict the operational reinforcing modulus of a curvy inserted CNT. Such a modulus was then applied within a micro mechanics case in order to determine the modulus of a polymer reinforced distributed with curvy CNTs. They figured out that even minor CNT curvature considerably lessens the reinforcement compared to conventional CNTs, and so on.

This paper is organized as follows. The properties of functionally graded carbon nanotube-reinforced composite (FG-CNTRC) plate is given in Section 2. Based on C^0-type of Shi's third-order shear deformation theory (C^0-STSDT), the finite element formulation for plate is briefly introduced in Section 3. To highlight the effectiveness of this element in analyzing the linear and nonlinear behaviors of FG-CNTRC plate structures, several numerical examples are thoroughly explored in Section 4. Finally, conclusions are drawn in Section 5.

2 Properties of Functionally Graded Carbon Nanotube-Reinforced Composite (FG-CNTRC) Plate

Four types UD, FGV, FGO and FGX of CNTs are shown in Figure 1, which can be expressed as

$$V_{CNT} = \begin{cases} V^*_{CNT} & \text{(UD)} \\ (1+2z/h)V^*_{CNT} & \text{(FGV)} \\ 2(1-2|z|/h)V^*_{CNT} & \text{(FGO)} \\ 2(2|z|/h)V^*_{CNT} & \text{(FGX)} \end{cases} \tag{1}$$

in which

$$V^*_{CNT} = \frac{\omega_{CNT}}{\omega_{CNT} + (\rho_{CNT}/\rho_m) - (\rho_{CNT}/\rho_m)\,\omega_{CNT}} \tag{2}$$

Where ρ_{CNT} and ρ_m are the density of CNTs and the matrix, ω_{CNT} is the mass fraction of the CNTs. Based on the rule of extended mixtures, the material properties of CNTs are written as [50]

$$E_{11} = \eta_1 V_{CNT} E_{11}^{CNT} + V_m E_m \tag{3}$$

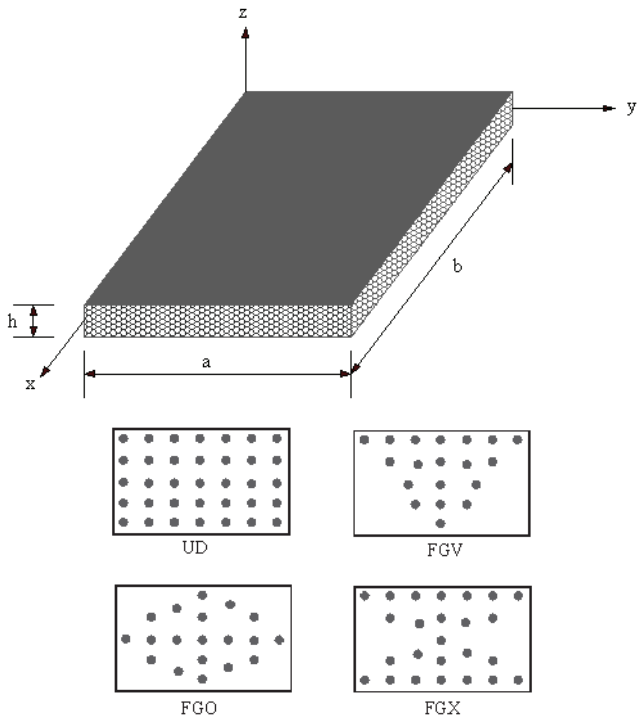

Figure 1 Configuration of carbon nanotube reinforced composite plate.

Table 1 The efficiency parameters of CNTs [50]

V^*_{CNT}	η_1	η_2	η_3
0.11	0.149	0.934	0.934
0.14	0.150	0.941	0.941
0.17	0.140	1.381	1.381

$$\eta_2/E_{22} = V_{CNT}/E_{22}^{CNT} + V_m/E_m \tag{4}$$

$$\eta_3/G_{12} = V_{CNT}/G_{12}^{CNT} + V_m/G_m \tag{5}$$

with G_m and E_m recall the shear modulus and Young's modulus of the isotropic matrix; G_{12}^{CNT} and E_{11}^{CNT}, E_{22}^{CNT} are called the shear modulus and Young's modulus of CNTs, η_1, η_2 and η_3 are efficiency parameters of CNTs as introduced in Table 1 [50]. V_m and V_{CNT} are called the matrix and CNT volume fractions and note that $V_{CNT} + V_m = 1$.

Similarly, Poisson's ratio ν_{12} is given as follows

$$\nu_{12} = V^*_{CNT}\nu_{12}^{CNT} + V_m\nu_m \tag{6}$$

3 Finite Element Formulation Based on C^0-STSDT for Plate

According to the theory of Shi [47], the displacement field can be described in terms of C^0-higher-order shear deformation theory and seven unknown variables as follows

$$u(x,y,z) = u_0(x,y) + \left(\frac{1}{4}z - \frac{5}{3h^2}z^3\right)\phi_x^b + \frac{5}{4}\left(z - \frac{4}{3h^2}z^3\right)\phi_x^s(x,y) \tag{7}$$

$$v(x,y,z) = v_0(x,y) + \left(\frac{1}{4}z - \frac{5}{3h^2}z^3\right)\phi_y^b + \frac{5}{4}\left(z - \frac{4}{3h^2}z^3\right)\phi_y^s(x,y) \tag{8}$$

$$w(x,y,z) = w_0(x,y) \tag{9}$$

It can be seen that the present theory is composed of seven unknowns including three axial and transverse displacements, four rotations due to the bending and shear effects as shown in Figure 2. The vector of Green-Lagrangian strain can be given as follows

$$\begin{Bmatrix} \varepsilon_x \\ \varepsilon_y \\ \varepsilon_{xy} \\ \gamma_{yz} \\ \gamma_{xz} \end{Bmatrix} = \begin{Bmatrix} \dfrac{\partial u}{\partial x} + \dfrac{1}{2}\left(\dfrac{\partial u}{\partial x}\right)^2 + \dfrac{1}{2}\left(\dfrac{\partial v}{\partial x}\right)^2 + \dfrac{1}{2}\left(\dfrac{\partial w}{\partial x}\right)^2 \\ \dfrac{\partial v}{\partial y} + \dfrac{1}{2}\left(\dfrac{\partial u}{\partial y}\right)^2 + \dfrac{1}{2}\left(\dfrac{\partial v}{\partial y}\right)^2 + \dfrac{1}{2}\left(\dfrac{\partial w}{\partial y}\right)^2 \\ \dfrac{\partial u}{\partial y} + \dfrac{\partial v}{\partial x} + \dfrac{\partial u}{\partial x}\dfrac{\partial u}{\partial y} + \dfrac{\partial v}{\partial x}\dfrac{\partial v}{\partial y} + \dfrac{\partial w}{\partial x}\dfrac{\partial w}{\partial y} \\ \dfrac{\partial v}{\partial z} + \dfrac{\partial w}{\partial y} + \dfrac{\partial u}{\partial y}\dfrac{\partial u}{\partial z} + \dfrac{\partial v}{\partial y}\dfrac{\partial v}{\partial z} + \dfrac{\partial w}{\partial y}\dfrac{\partial w}{\partial z} \\ \dfrac{\partial u}{\partial z} + \dfrac{\partial w}{\partial x} + \dfrac{\partial u}{\partial x}\dfrac{\partial u}{\partial z} + \dfrac{\partial v}{\partial x}\dfrac{\partial v}{\partial z} + \dfrac{\partial w}{\partial x}\dfrac{\partial w}{\partial z} \end{Bmatrix} \tag{10}$$

By using the Von Karman assumptions which imply that derivatives of *u* and *v* with respect to *x*, *y* and *z* are small and noting that *w* is independent of *z*, the above Green-Lagrangian's strain can be rewritten into a summation of nonlinear strains in plain and linear transverse shear strains in terms of the

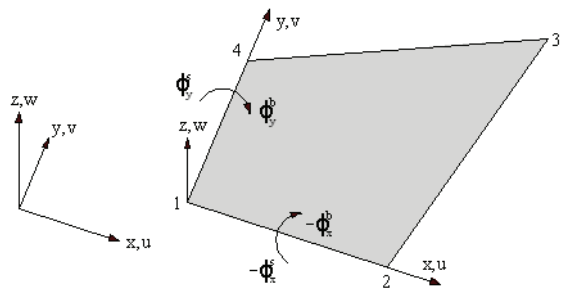

Figure 2 The positive directions of the displacement components.

mid-plane deformations. Specifically, the nonlinear strains in plain and the linear transverse shear strains are expressed in matrix form

$$\begin{Bmatrix} \boldsymbol{\varepsilon} \\ \boldsymbol{\gamma} \end{Bmatrix} = \begin{Bmatrix} \boldsymbol{\varepsilon}^{(\mathbf{0})} \\ \boldsymbol{\gamma}^{(\mathbf{0})} \end{Bmatrix} + \mathrm{z} \begin{Bmatrix} \boldsymbol{\varepsilon}^{(\mathbf{1})} \\ \mathbf{0} \end{Bmatrix} + \mathbf{z}^2 \begin{Bmatrix} \mathbf{0} \\ \boldsymbol{\gamma}^{(\mathbf{2})} \end{Bmatrix} + \mathbf{z}^3 \begin{Bmatrix} \boldsymbol{\varepsilon}^{(\mathbf{3})} \\ \mathbf{0} \end{Bmatrix} \tag{11}$$

with

$$\boldsymbol{\varepsilon}^{(0)} = \boldsymbol{\varepsilon}_L^{(0)} + \boldsymbol{\varepsilon}_{NL}^{(0)} = \underbrace{\begin{Bmatrix} u_{0,x} \\ v_{0,y} \\ u_{0,y} + v_{0,x} \end{Bmatrix}}_{\text{linear part}} + \underbrace{\begin{Bmatrix} \frac{1}{2} w_{,x}^2 \\ \frac{1}{2} w_{,y}^2 \\ w_{,y} w_{,x} \end{Bmatrix}}_{\text{nonlinear part}} ;$$

$$\boldsymbol{\varepsilon}^{(1)} = \frac{1}{4} \begin{Bmatrix} \left(5\phi_{x,x}^s + \phi_{x,x}^b\right) \\ \left(5\phi_{y,y}^s + \phi_{y,y}^b\right) \\ \left(5\phi_{x,y}^s + 5\phi_{y,x}^s + \phi_{x,y}^b + \phi_{y,x}^b\right) \end{Bmatrix};$$

$$\boldsymbol{\varepsilon}^{(3)} = \frac{-5}{3h^2} \begin{Bmatrix} \phi_{x,x}^s + \phi_{x,x}^b \\ \phi_{y,y}^s + \phi_{y,y}^b \\ \phi_{x,y}^s + \phi_{x,y}^b + \phi_{y,x}^s + \phi_{y,x}^b \end{Bmatrix} \tag{12}$$

$$\boldsymbol{\gamma}^{(0)} = \begin{Bmatrix} \frac{5}{4}\phi_y^s + \frac{1}{4}\phi_y^b + w_{,y} \\ \frac{5}{4}\phi_x^s + \frac{1}{4}\phi_x^b + w_{,x} \end{Bmatrix}; \quad \boldsymbol{\gamma}^{(2)} = \frac{-5}{h^2} \begin{Bmatrix} \phi_y^s + \phi_y^b \\ \phi_x^s + \phi_x^b \end{Bmatrix} \tag{13}$$

Note that $\boldsymbol{\varepsilon}^{(0)}$ is called the membrane strains; $\boldsymbol{\varepsilon}^{(1)}$, $\boldsymbol{\varepsilon}^{(3)}$ are called the bending strains as well as $\boldsymbol{\gamma}^{(0)}$, $\boldsymbol{\gamma}^{(2)}$ are also called as two components of

transverse shear strains in this study. It must be also noted in all equations that author has denoted *L* or *NL* to indicate the linear or nonlinear part.

The constitutive relation for functionally graded plate can be defined as below

$$\begin{Bmatrix} \sigma_{xx} \\ \sigma_{yy} \\ \sigma_{xy} \\ \tau_{xz} \\ \tau_{yz} \end{Bmatrix} = \begin{bmatrix} Q_{11} & Q_{12} & 0 & 0 & 0 \\ Q_{21} & Q_{22} & 0 & 0 & 0 \\ 0 & 0 & Q_{66} & 0 & 0 \\ 0 & 0 & 0 & Q_{55} & 0 \\ 0 & 0 & 0 & 0 & Q_{44} \end{bmatrix} \begin{Bmatrix} \varepsilon_{xx} \\ \varepsilon_{yy} \\ \varepsilon_{xy} \\ \gamma_{xz} \\ \gamma_{yz} \end{Bmatrix} \tag{14}$$

with the material constants are given by

$$\begin{aligned} &Q_{11} = Q_{22} = E(z)/[1-\nu^2(z)], \quad Q_{12} = Q_{21} = \nu(z)E(z)/[1-\nu^2(z)], \\ &Q_{44} = Q_{55} = Q_{66} = E(z)/2[1+\nu(z)] \end{aligned} \tag{15}$$

Through the thickness of plate, the constitutive relation as above can be rewritten

$$\boldsymbol{\sigma}^* = \mathbf{D}^* \boldsymbol{\varepsilon}^* \tag{16}$$

in which

$$\mathbf{D}^* = \begin{bmatrix} \mathbf{D}_b^* & 0 \\ 0 & \mathbf{D}_s^* \end{bmatrix}, \quad \text{with } \mathbf{D}_b^* = \begin{bmatrix} \mathbf{A} & \mathbf{B} & \mathbf{E} \\ \mathbf{B} & \mathbf{D} & \mathbf{F} \\ \mathbf{E} & \mathbf{F} & \mathbf{H} \end{bmatrix}, \quad \mathbf{D}_s^* = \begin{bmatrix} \mathbf{A}^s & \mathbf{B}^s \\ \mathbf{B}^s & \mathbf{D}^s \end{bmatrix} \tag{17}$$

and

$$\boldsymbol{\sigma}^* = \begin{bmatrix} \mathbf{N} \\ \mathbf{M} \\ \mathbf{T} \\ \mathbf{S} \\ \mathbf{R} \end{bmatrix}, \boldsymbol{\varepsilon}^* = \begin{bmatrix} \boldsymbol{\varepsilon}^{(0)} \\ \boldsymbol{\varepsilon}^{(1)} \\ \boldsymbol{\varepsilon}^{(3)} \\ \boldsymbol{\gamma}^{(0)} \\ \boldsymbol{\gamma}^{(2)} \end{bmatrix} \tag{18}$$

N is the normal forces, **M** is bending moments, **T** is higher-order moments, **S** and **R** are related to shear forces, respectively.

$$(\mathbf{A}, \mathbf{B}, \mathbf{D}, \mathbf{E}, \mathbf{F}, \mathbf{H}) = \int_{-h/2}^{h/2} (1, z, z^2, z^3, z^4, z^6) \begin{bmatrix} Q_{11} & Q_{12} & 0 \\ Q_{21} & Q_{22} & 0 \\ 0 & 0 & Q_{66} \end{bmatrix} dz \tag{19}$$

$$(\mathbf{A}^s, \mathbf{B}^s, \mathbf{D}^s) = \int_{-h/2}^{h/2} \left(1, z^2, z^4\right) \begin{bmatrix} Q_{55} & 0 \\ 0 & Q_{44} \end{bmatrix} dz \tag{20}$$

From the C^0-STSDT, the strains can be approximated by

$$\boldsymbol{\varepsilon}_L^{(0)} = \mathbf{B}_1^L\mathbf{d}; \quad \boldsymbol{\varepsilon}_{NL}^{(0)} = \mathbf{B}_1^{NL}\mathbf{d}; \quad \boldsymbol{\varepsilon}^{(1)} = \mathbf{B}_2\mathbf{d}; \quad \boldsymbol{\varepsilon}^{(3)} = \mathbf{B}_3\mathbf{d} \tag{21}$$

$$\boldsymbol{\gamma}^{(0)} = \mathbf{B}_4\mathbf{d}; \quad \boldsymbol{\gamma}^{(2)} = \mathbf{B}_5\mathbf{d} \tag{22}$$

In which

$$\mathbf{d} = \begin{bmatrix}\mathbf{d}_1 & \mathbf{d}_2 & \mathbf{d}_3 & \mathbf{d}_4\end{bmatrix}^{\mathrm{T}}; \quad \mathbf{d}_i = \begin{bmatrix}u_{0i} & v_{0i} & w_i & \phi_{xi}^s & \phi_{yi}^s & \phi_{xi}^b & \phi_{yi}^b\end{bmatrix}^{\mathrm{T}} \tag{23}$$

These two quantities $\mathbf{d}_i$ and $\mathbf{d}$ provide information about the number of degrees of freedom for each node as well as that of each element. All matrices $\mathbf{B}_1^L$, $\mathbf{B}_1^{NL}$, $\mathbf{B}_2$, $\mathbf{B}_3$, $\mathbf{B}_4$ and $\mathbf{B}_5$ can be described as below

$$\mathbf{B}_1^L = \sum_{i=1}^{4}\begin{bmatrix}\mathbf{N}_{i,x} & 0 & 0 & 0 & 0 & 0 & 0\\ 0 & \mathbf{N}_{i,y} & 0 & 0 & 0 & 0 & 0\\ \mathbf{N}_{i,y} & \mathbf{N}_{i,x} & 0 & 0 & 0 & 0 & 0\end{bmatrix};$$

$$\mathbf{B}_1^{NL} = \mathbf{H}_{geo}\mathbf{G} = \sum_{i=1}^{4}\mathbf{H}_{geo_i}\mathbf{G}_i \tag{24}$$

$$\mathbf{H}_{geo_i} = \begin{bmatrix}\mathbf{N}_{i,x}w_i & 0\\ 0 & \mathbf{N}_{i,y}w_i\\ \mathbf{N}_{i,y}w_i & \mathbf{N}_{i,x}w_i\end{bmatrix}, \quad \mathbf{G}_i = \begin{bmatrix}0 & 0 & \mathbf{N}_{i,x} & 0 & 0 & 0 & 0\\ 0 & 0 & \mathbf{N}_{i,y} & 0 & 0 & 0 & 0\end{bmatrix} \tag{25}$$

$$\mathbf{B}_2 = \frac{1}{4}\sum_{i=1}^{4}\begin{bmatrix}0 & 0 & 0 & 5\mathbf{N}_{i,x} & 0 & \mathbf{N}_{i,x} & 0\\ 0 & 0 & 0 & 0 & 5\mathbf{N}_{i,y} & 0 & \mathbf{N}_{i,y}\\ 0 & 0 & 0 & 5\mathbf{N}_{i,y} & 5\mathbf{N}_{i,x} & \mathbf{N}_{i,y} & \mathbf{N}_{i,x}\end{bmatrix} \tag{26}$$

$$\mathbf{B}_3 = -\frac{5}{3h^2}\sum_{i=1}^{4}\begin{bmatrix}0 & 0 & 0 & \mathbf{N}_{i,x} & 0 & \mathbf{N}_{i,x} & 0\\ 0 & 0 & 0 & 0 & \mathbf{N}_{i,y} & 0 & \mathbf{N}_{i,y}\\ 0 & 0 & 0 & \mathbf{N}_{i,y} & \mathbf{N}_{i,x} & \mathbf{N}_{i,y} & \mathbf{N}_{i,x}\end{bmatrix} \tag{27}$$

$$\mathbf{B}_4 = \sum_{i=1}^{4}\begin{bmatrix}0 & 0 & \mathbf{N}_{i,y} & 0 & \frac{5}{4} & 0 & \frac{1}{4}\\ 0 & 0 & \mathbf{N}_{i,x} & \frac{5}{4} & 0 & \frac{1}{4} & 0\end{bmatrix};$$

$$\mathbf{B}_5 = -\frac{5}{h^2}\sum_{i=1}^{4}\begin{bmatrix}0 & 0 & 0 & 0 & 1 & 0 & 1\\ 0 & 0 & 0 & 1 & 0 & 1 & 0\end{bmatrix} \tag{28}$$

$$\mathbf{N} = \begin{bmatrix}N_1 & N_2 & N_3 & N_4\end{bmatrix} \text{ is clearly shape function vector} \tag{29}$$

The tangent stiffness matrix is introduced

$$\mathbf{K} = \mathbf{K}_L + \mathbf{K}_{NL} + \mathbf{K}_g \tag{30}$$

where $\mathbf{K}_L$ and $\mathbf{K}_{NL}$ present the linear and nonlinear stiffness matrices and $\mathbf{K}_g$ is the geometric stiffness matrix. They are obtained as follows

$$\mathbf{K}_L = \mathbf{B}_L^T \mathbf{D}^* \mathbf{B}_L \tag{31}$$

$$\mathbf{K}_{NL} = \mathbf{B}_{NL}^T \mathbf{D}^* \mathbf{B}_{NL} \tag{32}$$

$$\mathbf{K}_g = \mathbf{G}^T \tilde{\mathbf{N}} \mathbf{G} \tag{33}$$

with

$$\mathbf{B}_L = \begin{bmatrix} \mathbf{B}_1^L \\ \mathbf{B}_2 \\ \mathbf{B}_3 \\ \mathbf{B}_4 \\ \mathbf{B}_5 \end{bmatrix}, \quad \mathbf{B}_{NL} = \begin{bmatrix} \mathbf{B}_1^{NL} \\ \mathbf{0} \\ \mathbf{0} \\ \mathbf{0} \\ \mathbf{0} \end{bmatrix}, \quad \tilde{\mathbf{N}} = \begin{bmatrix} N_x & N_{xy} \\ N_{xy} & N_y \end{bmatrix} \tag{34}$$

Based on the Total Lagrangian approach, the internal forces at the loop *t* computed from the stress state in the structures can be rewritten as

$${}^t\mathbf{F} = \int_\Omega (\mathbf{B}_L + \mathbf{B}_{NL}) {}^t\boldsymbol{\sigma}^* d\Omega \tag{35}$$

where the result of stress after the ith iteration is

$${}^t\boldsymbol{\sigma}_{i+1}^* = {}^t\boldsymbol{\sigma}_i^* + {}^t\Delta\boldsymbol{\sigma}^* \tag{36}$$

Finally, the nonlinear equations can be given as

$${}^t\mathbf{K}_T \Delta\mathbf{d} = {}^{t+\Delta t}\mathbf{P} - {}^t\mathbf{F} \tag{37}$$

where ${}^{t+\Delta t}\mathbf{P}$ is the external force at time $t + \Delta t$.

4 Numerical Results

We verify the reliability of the proposed element through various examples related to FG-CNTRC plate structures. Unless stated otherwise, material properties of matrix, PmPV, are expressed to be $E_m = 2.1$ Gpa, $\nu_m = 0.34$ at the room temperature [3, 51], and the reinforcements (10,10) SWCNTs [52] are given by $E_{11}^{CNT} = 5.6466$ Tpa, $E_{22}^{CNT} = 7.08$ Tpa, $G_{12}^{CNT} = 1.9445$ Tpa, $\nu_{12}^{CNT} = 0.175$. In addition, $G_{12} = G_{13} = G_{23}$ is assumed in this study. Furthermore, the boundary conditions are defined as follows:

Clamped (C): $u_o = v_o = w_o = \phi_x^s = \phi_x^b = \phi_y^s = \phi_y^b = 0$

Simply supported (S): for upper and lower edges: $u_o = w_o = \phi_y^s = \phi_y^b = 0$, for left and right edges: $v_o = w_o = \phi_x^s = \phi_x^b = 0$.

Table 2 Comparison of normalized central deflection for the simply supported FG-CNTRC square plate with $V^*_{CNT} = 0.17$

Types	Ansys [52]	FEM [52]	CS-DSG3 [53]	IGA [54]	Analytical [55]	Present
FG-X	0.5141	0.5132	0.5144	0.5126	0.5156	0.5148
FG-O	1.4110	1.4160	1.4153	1.4426	1.4120	1.4152
FG-V	1.0810	1.0820	1.0834	1.1010	1.0820	1.0830
UD	0.7521	0.7515	0.7524	0.7588	0.7523	0.7532

4.1 Linear Bending Analysis

The static behavior of an FG-CNTRC plate under uniformly distributed load $q = 10^5(N/m^2)$ with three values of CNTs volume fraction ($V^*_{CNT} = 0.11/0.14/0.17$) is studied in this example. Table 2 compares the normalized central deflection of the (SSSS) FG-CNTRC square plates with the volume fraction of CNTs $V^*_{CNT} = 0.17$ and the length-to-thickness ratio $a/h = 50$ by six different methods, including commercial software package Ansys [52], standard finite element method [52], CS-DSG3 [53], IGA [54], analytical [55] and C^0-STSDT. In this study, this element related to Shi's theory (STSDT) under C^0-type with seven degrees-of-freedom per node while IGA [54] with the same degrees-of-freedom per node used the other third-order shear deformation theory. It can be observed that the paper's results agree well with other solutions.

Table 3 also presents the normalized central deflection for the FG-CNTRC square plates with the length-to-thickness ratio $a/h = 20$ and three values of the volume fraction of CNTs under two boundary conditions (SSSS) & (CCCC) in comparison with those of the CS-DSG3 [53] and the IGA's results [54]. It is observed that the present results match well with other solutions. It is also found that an increase in the volume fraction $V^*_{CNT}$of CNTs leads a decrease in the normalized central deflection of FG-CNTRC plates. With types FG-O and FG-X, the FG-CNTRC plate have the smallest and greatest stiffness because of the greatest and smallest deflections of them.

The effects of CNT volume fraction and length-to-thickness ratio *a/h* on the normalized central deflection for full types of FG-CNTRC square plates are presented in Table 4. The results of the proposed element are compared with other results related to the commercial software package Ansys [52] as well as the standard finite element method in [52]. It can be seen that three groups of results match very well. Once again, It can be found that the central deflection of the plates is greatly influenced by the change in volume fraction of CNT. Specifically, this deflection will decrease to 30% when only 6% of

Table 3 Comparison of normalized central deflection for the FG-CNTRC square plates with two boundary conditions (SSSS) & (CCCC) and three values of V^*_{CNT}

V^*_{CNT}	Types	SSSS			CCCC		
		CS-DSG3	IGA	Present	CS-DSG3	IGA	Present
0.11	FG-X	0.02664	0.02594	0.02704	0.01114	0.01016	0.01149
	FG-O	0.06116	0.06179	0.06153	0.01824	0.01747	0.01860
	FG-V	0.04846	0.04854	0.04881	0.01557	0.01472	0.01592
	UD	0.03589	0.03551	0.03631	0.01302	0.01205	0.01338
0.14	FG-X	0.02214	0.02140	0.02252	0.00999	0.00910	0.01033
	FG-O	0.05013	0.05040	0.05051	0.01565	0.01490	0.01600
	FG-V	0.03976	0.03962	0.04013	0.01352	0.01270	0.01386
	UD	0.02955	0.02900	0.02994	0.01150	0.01056	0.01185
0.17	FG-X	0.01715	0.01675	0.01740	0.00707	0.00749	0.00729
	FG-O	0.03995	0.04031	0.04017	0.01175	0.01131	0.01198
	FG-V	0.03153	0.03166	0.03175	0.00999	0.00951	0.01021
	UD	0.02324	0.02300	0.02351	0.00833	0.00873	0.00856

the volume fraction of CNT is increased. Note that the central deflections of two types FG-V and FG-O plates are larger than those of two types UD and FG-X though all types of plates have the same mass fraction of the CNT. By changing the distribution of reinforcements, the stiffness of plates can be affected, and this action is expected to get the desired stiffness of these structures in reality. Furthermore, if these reinforcements are distributed on the bottom or top surface, the plates will achieve better stiffness than in other cases.

According to Figure 3, the normalized central axial stresses $\bar{\sigma}_{xx} = \sigma_{xx}h^2/(|q|a^2)$ of FG-CNTRC square plates along thickness direction with length-to-thickness ratio $a/h = 50$ and CNT volume fraction $V^*_{CNT} = 0.17$ based on the proposed element are compared with the results of [52]. Figure 3(a) under boundary condition (CCCC) as well as Figure 3(b) under boundary condition (SSSS) show that the paper's results match well with other results [52]. The central axial stress distribution in four types UD, FG-O, FG-V and FG-X CNTRC plates will differ as shown throughout the thickness. The axial stress equals zero at the bottom of FG-V CNTRC plate as well as the value of this quantity equals zero on both the top and bottom surface of the FG-O CNTRC plate.

Table 4 The effects of length-to-thickness ratio *a/h* and volume fraction of CNT on the normalized central deflection for full types of FG-CNTRC square plates with two boundary conditions (SSSS) & (CCCC)

V^*_{CNT}		Types	SSSS			CCCC		
			Ansys	FEM	Present	Ansys	FEM	Present
0.11	10	FG-X	0.00318	0.00318	0.00318	0.00210	0.00211	0.00210
		FG-O	0.00522	0.00523	0.00522	0.00251	0.00251	0.00251
		FG-V	0.00446	0.00446	0.00446	0.00235	0.00235	0.00235
		UD	0.00374	0.00374	0.00374	0.00223	0.00223	0.00222
	20	FG-X	0.02703	0.02701	0.02705	0.01150	0.01150	0.01150
		FG-O	0.06136	0.06155	0.06153	0.01856	0.01860	0.01861
		FG-V	0.04876	0.04879	0.04882	0.01591	0.01593	0.01593
		UD	0.03629	0.03628	0.03632	0.01338	0.01339	0.01338
	50	FG-X	0.79150	0.79000	0.79187	0.19000	0.18940	0.19079
		FG-O	2.15000	2.15700	2.15704	0.47050	0.47190	0.47303
		FG-V	1.65200	1.65300	1.65409	0.36530	0.36490	0.36589
		UD	1.15500	1.15500	1.15639	0.26180	0.26180	0.26271
0.14	10	FG-X	0.00284	0.00284	0.00284	0.00198	0.00198	0.00197
		FG-O	0.00451	0.00453	0.00451	0.00231	0.00231	0.00231
		FG-V	0.00389	0.00389	0.00388	0.00218	0.00218	0.00217
		UD	0.00331	0.00330	0.00330	0.00209	0.00209	0.00208
	20	FG-X	0.02258	0.02256	0.02253	0.01035	0.01036	0.01033
		FG-O	0.05053	0.05070	0.05051	0.01600	0.01604	0.01600
		FG-V	0.04021	0.04025	0.04013	0.01388	0.01390	0.01387
		UD	0.03002	0.03001	0.02995	0.01188	0.01188	0.01185
	50	FG-X	0.62840	0.62710	0.62618	0.15660	0.15600	0.15743
		FG-O	1.73200	1.73800	1.73178	0.37970	0.38050	0.38005
		FG-V	1.32500	1.32600	1.32174	0.29580	0.29550	0.29527
		UD	0.91820	0.91750	0.91573	0.21310	0.21310	0.21353
0.17	10	FG-X	0.00201	0.00201	0.00201	0.00132	0.00132	0.00132
		FG-O	0.00337	0.00338	0.00337	0.00159	0.00160	0.00159
		FG-V	0.00286	0.00286	0.00286	0.00148	0.00149	0.00148
		UD	0.00239	0.00239	0.00239	0.00141	0.00141	0.00141

(*Continued*)

Table 4 Continued

V^*_{CNT}	Types		SSSS			CCCC		
			Ansys	FEM	Present	Ansys	FEM	Present
	20	FG-X	0.01738	0.01737	0.01741	0.00729	0.00729	0.00729
		FG-O	0.04007	0.04020	0.04017	0.01195	0.01198	0.01198
		FG-V	0.03171	0.03174	0.03175	0.01020	0.01021	0.01021
		UD	0.02349	0.02348	0.02351	0.00856	0.00856	0.00856
	50	FG-X	0.51410	0.51320	0.51486	0.12270	0.12230	0.12313
		FG-O	1.41100	1.41600	1.41521	0.30790	0.30850	0.30930
		FG-V	1.08100	1.08200	1.08301	0.23860	0.23840	0.23910
		UD	0.75210	0.75150	0.75324	0.16990	0.16980	0.17048

With four values (5, 10, 50 & 100) of length-to-thickness ratio *a/h*, the effect of them on the normalized central axial stresses in two types FG-V and FG-O CNTRC square plates with CNT volume fraction $V^*_{CNT} = 0.17$ under two boundary conditions (CCCC) & (SSSS) are also presented in Figures 4(a) and 4(b) respectively.

Next, the UD, FG-V, FG-O and FG-X CNTRC skew plates ($a/b = 1$) with three values of skew angle 30°, 45° and 60° are studied in this section. By changing the value of skew angle and the value of length-to-thickness ratio *a/h*, the normalized central deflection for the FG-CNTRC skew plates with three values of the volume fraction of CNTs ($V^*_{CNT} = 0.11/0.14/0.17$) under two boundary conditions (SSSS) & (CCCC) are given as Table 5.

On the other hand, based on the stability of the proposed element, the normalized central axial stresses $\bar{\sigma}_{xx} = \sigma_{xx}h^2/(|q|a^2)$ of FG-CNTRC skew plates along thickness direction with two values of length-to-thickness ratio $a/h = 10$ & 50; three values of skew angle 30°, 45° & 60°; two types FG-V & FG-O under CNT volume fraction $V^*_{CNT} = 0.11$ are shown in Figures 5(a) and 5(b) for boundary condition (SSSS) and in Figures 5(c) and 5(d) for boundary condition (CCCC) with expectations as a further reference data in the future.

4.2 Nonlinear Bending Analysis

In this section, the nonlinear bending analysis of FG-CNTRC square plates are presented in details with the expectation of the efficiency based on this proposed element. Two types UD and FG-V CNTRC are used to study the

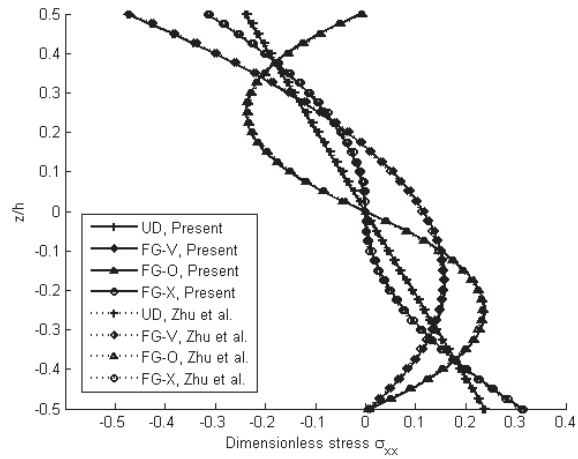

(a) $a/h = 50$, $V^*_{CNT} = 0.17$, (CCCC)

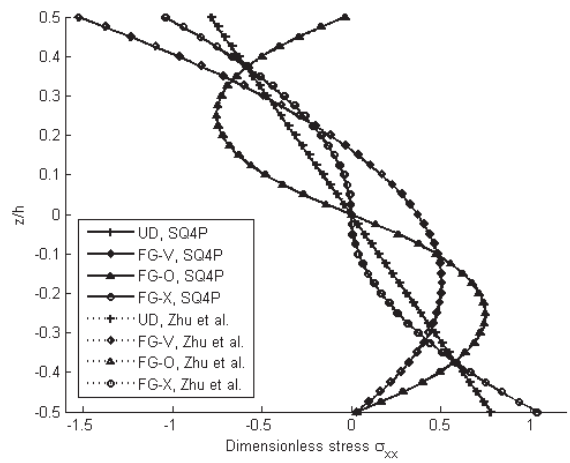

(b) $a/h = 50$, $V^*_{CNT} = 0.17$, (SSSS)

Figure 3 The normalized central axial stresses in the FG-CNTRC plates under a uniform load.

values of nonlinear deflection. Under three values of CNT volume fraction ($V^*_{CNT} = 0.11/0.14/0.17$), the load-deflection curves for UD and FG-V CNTRC square plates with length-to-thickness ratio $a/h = 10$ are shown as Figures 6(a)–6(c). It can be seen that the results achieved by paper's elements

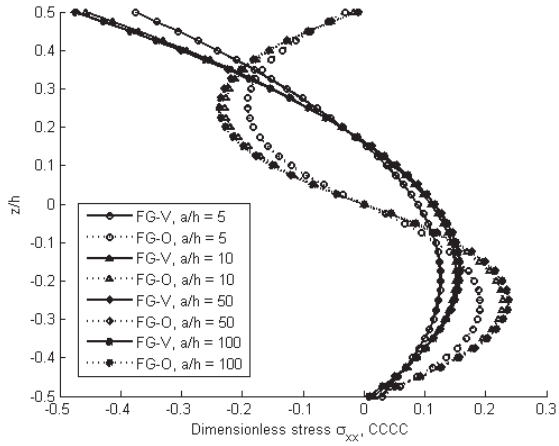

(a) $V^*_{CNT} = 0.17$, (CCCC)

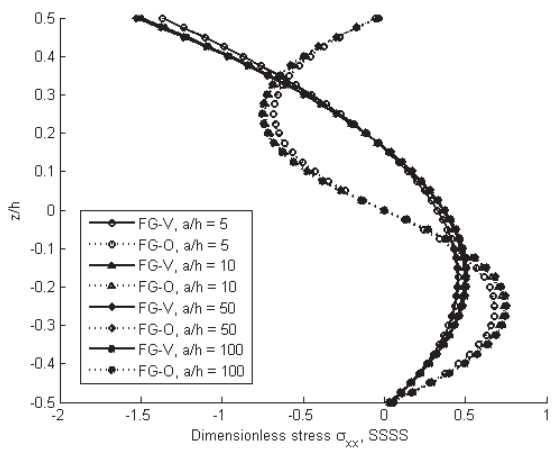

(b) $V^*_{CNT} = 0.17$, (SSSS)

Figure 4 The effect of length-to-thickness ratio *a/h* on the normalized central axial stresses.

match well with the results of Shen in [50]. The results obtained by us are slightly smaller than those of Shen [50] and the difference is negligible.

Now, the nonlinear bending analysis of FG-CNTRC skew plates are presented in this paper related to C^0-STSDT. Three values of skew angle 30°, 45° & 60°; full types of FG-CNTRC; three values 0.11, 0.14 & 0.17 of CNT volume fraction; three values 10, 15 & 20 of length-to-thickness ratio *a/h*; three values width-to-length ratio $b/a = 0.5$, 1 & 2 as well as two types of

Table 5 The effects of CNT volume fraction, length-to-thickness ratio *a/h* and skew angle on the normalized central deflection for full types of FG-CNTRC skew plates $(a/b = 1)$ with two boundary conditions (SSSS) & (CCCC)

V^*_{CNT}	Types		SSSS			CCCC		
			30°	45°	60°	30°	45°	60°
0.11	10	FG-X	0.00315	0.00281	0.00191	0.00210	0.00189	0.00132
		FG-O	0.00475	0.00379	0.00227	0.00246	0.00217	0.00146
		FG-V	0.00416	0.00343	0.00213	0.00232	0.00206	0.00140
		UD	0.00362	0.00313	0.00205	0.00221	0.00199	0.00138
	20	FG-X	0.02745	0.02512	0.01730	0.01259	0.01300	0.01048
		FG-O	0.05398	0.04124	0.02327	0.01955	0.01883	0.01346
		FG-V	0.04470	0.03579	0.02115	0.01695	0.01665	0.01231
		UD	0.03536	0.03054	0.01958	0.01453	0.01476	0.01154
	50	FG-X	0.74358	0.64711	0.43835	0.21832	0.24817	0.23643
		FG-O	1.56392	1.12454	0.65014	0.51262	0.51736	0.39028
		FG-V	1.29370	0.96893	0.57617	0.40400	0.42144	0.33702
		UD	1.00266	0.81223	0.51600	0.29763	0.32719	0.28945
0.14	10	FG-X	0.00284	0.00257	0.00178	0.00197	0.00178	0.00125
		FG-O	0.00420	0.00346	0.00214	0.00228	0.00204	0.00139
		FG-V	0.00369	0.00312	0.00199	0.00215	0.00193	0.00132
		UD	0.00324	0.00287	0.00193	0.00208	0.00188	0.00132
	20	FG-X	0.02329	0.02191	0.01565	0.01136	0.01181	0.00966
		FG-O	0.04604	0.03669	0.02157	0.01707	0.01683	0.01249
		FG-V	0.03792	0.03154	0.01939	0.01491	0.01491	0.01134
		UD	0.02993	0.02678	0.01792	0.01296	0.01334	0.01069
	50	FG-X	0.60906	0.55049	0.38792	0.18023	0.20794	0.20546
		FG-O	1.33280	0.99462	0.59336	0.41953	0.43757	0.34957
		FG-V	1.08966	0.84734	0.51964	0.33058	0.35425	0.29788
		UD	0.83151	0.70230	0.46366	0.24368	0.27385	0.25408
0.17	10	FG-X	0.00198	0.00175	0.00118	0.00131	0.00117	0.00082
		FG-O	0.00306	0.00244	0.00146	0.00157	0.00139	0.00093
		FG-V	0.00266	0.00218	0.00134	0.00146	0.00129	0.00088
		UD	0.00231	0.00199	0.00130	0.00140	0.00126	0.00087

(*Continued*)

Table 5 Continued

V^*_{CNT}	Types		SSSS			CCCC		
			30°	45°	60°	30°	45°	60°
	20	FG-X	0.01752	0.01583	0.01073	0.00795	0.00814	0.00649
		FG-O	0.03511	0.02673	0.01504	0.01260	0.01214	0.00869
		FG-V	0.02883	0.02286	0.01337	0.01084	0.0106	0.00777
		UD	0.02279	0.01956	0.01245	0.00928	0.00941	0.00733
	50	FG-X	0.47777	0.40972	0.27273	0.14067	0.15864	0.14829
		FG-O	1.01566	0.72908	0.42226	0.33503	0.33782	0.25439
		FG-V	0.83531	0.61991	0.36592	0.26303	0.27248	0.21513
		UD	0.64789	0.52129	0.32919	0.19286	0.21124	0.18539

boundary condition (SSSS) & (CCCC) are used to achieve the load-deflection curves under uniform load as shown in Figures 7–9. In details, Figure 7a depicts four curves for four types UD, FG-V, FG-O & FG-X with skew angle 30°, $V^*_{CNT} = 0.11$, $a/h = 10$, $b/a = 1$ and boundary condition (SSSS). As linear bending, with types FG-X and FG-O, the FG-CNTRC skew plates have the greatest and smallest stiffness because of the smallest and greatest deflections of them. Figure 7b presents the effect of CNT volume fraction on the load-deflection curve for (SSSS) UD-CNTRC skew plate with skew angle 30°, length-to-thickness ratio $a/h = 10$. Obviously, when CNT volume fraction is increased, the stiffness of the structure also increases, leading to a decrease in the deflection. By changing the length-to-thickness ratio *a/h* or the width-to-length ratio *b/a*, the deflection-load curves of FGO-CNTRC skew plate with CNT volume fraction $V^*_{CNT} = 0.17$ and boundary condition (SSSS) are also plotted in Figures 7(c) and 7(d).

Furthermore, the effect of skew angle on the nonlinear bending behavior of FG-CNTRC skew plates are studied in details. With CNT volume fraction 0.11 and boundary condition (SSSS), the load-deflection curve of UD-CNTRC skew plate gradually decreases with increasing skew angle value as depicted in Figure 8(a). This comment is also repeated for FGX-CNTRC skew plate as shown in Figure 8(b), and obviously Figure 8(c) is a combination of them.

Similarly, by changing the boundary condition from (SSSS) to (CCCC), the effect of skew angle on the nonlinear bending behavior of FG-CNTRC skew plates are also presented in last research. The difference between type UD and type FGX of CNTRC skew plate is not significant as shown in

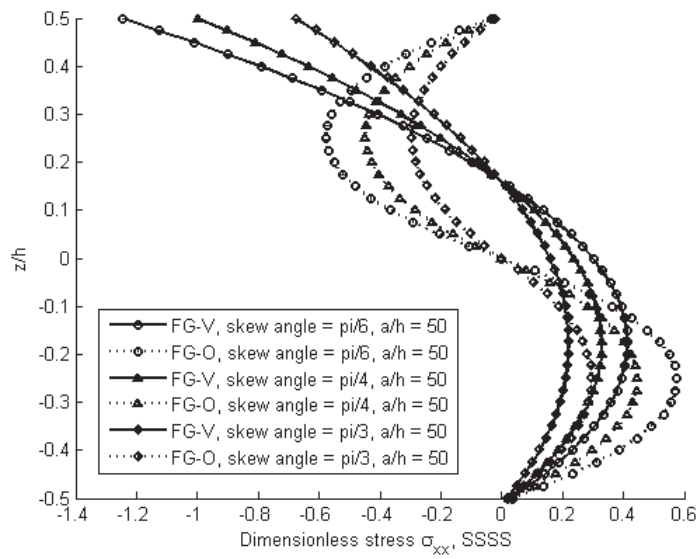

(a) $V^*_{CNT} = 0.11$, $a/h = 50$, (SSSS)

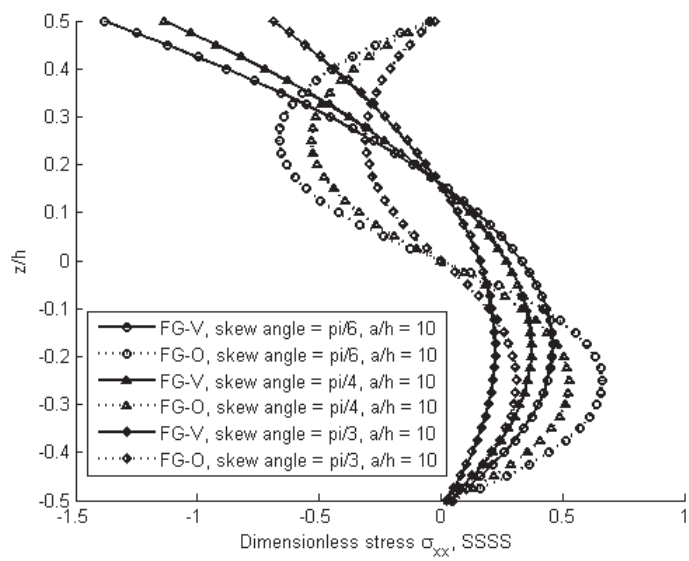

(b) $V^*_{CNT} = 0.11$, $a/h = 10$, (SSSS)

Figure 5 Continued

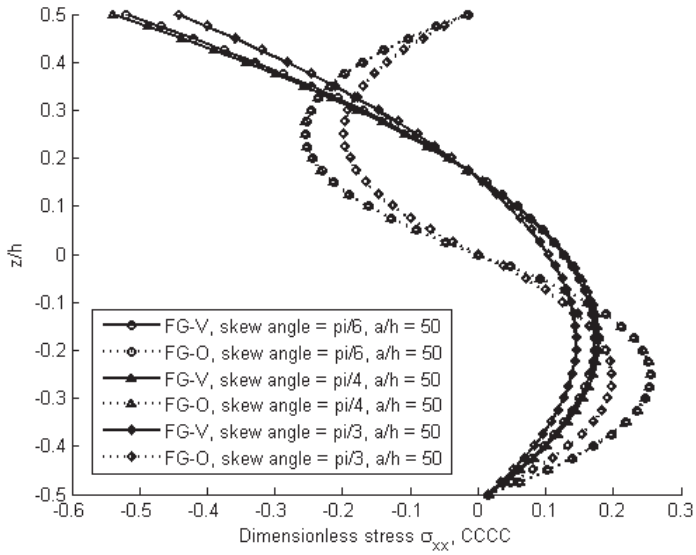

(c) $V^*_{CNT} = 0.11$, $a/h = 50$, (CCCC)

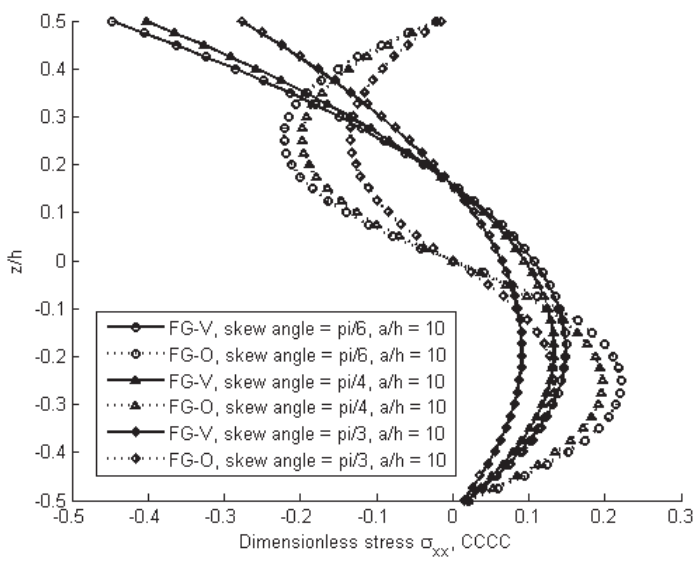

(d) $V^*_{CNT} = 0.11$, $a/h = 10$, (CCCC)

Figure 5 The effects of length-to-thickness ratio a/h, skew angle, type of FG and boundary condition on the normalized central axial stresses.

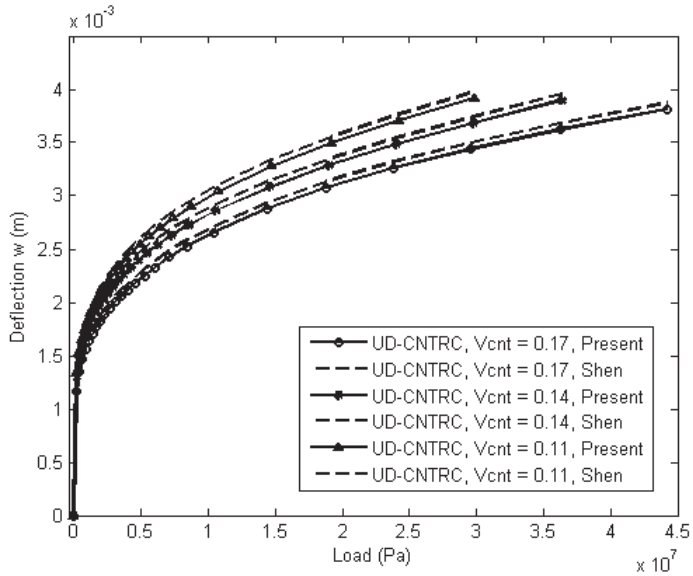

(a)

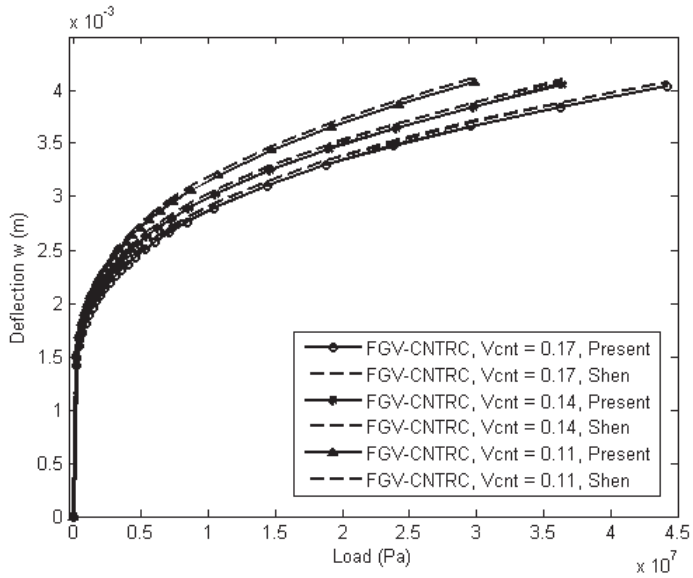

(b)

Figure 6 Continued

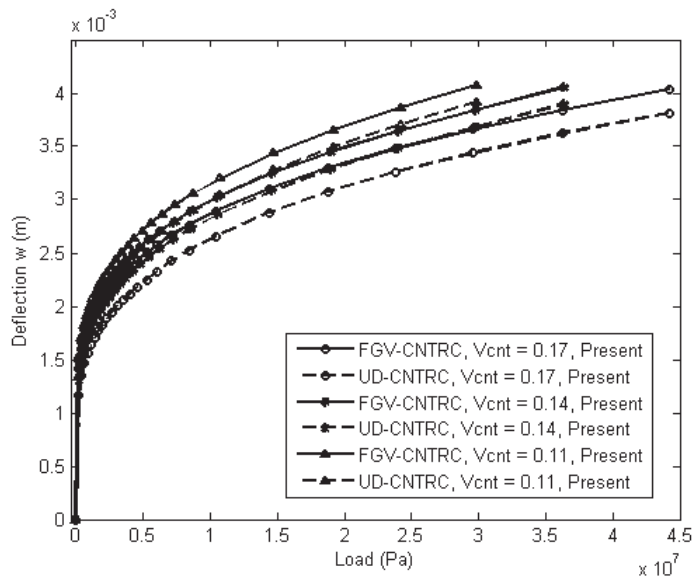

(c)

Figure 6 (a) Comparison for UD-CNTRC square plates, (b) comparison for FGV-CNTRC square plates and (c) six load-deflection curves for both UD and FGV-CNTRC square plates with $a/h = 10$.

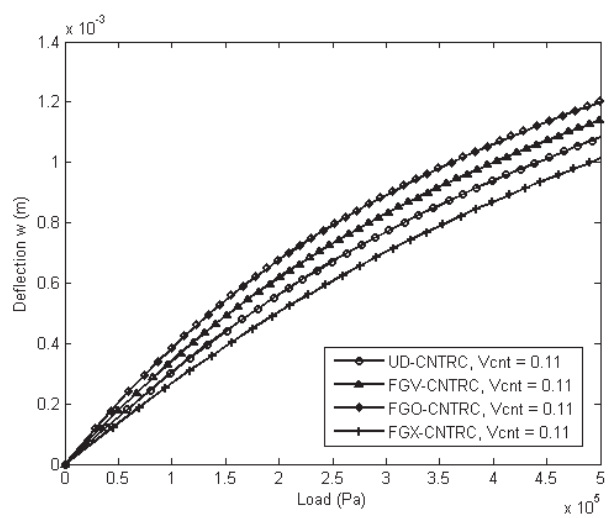

(a) Skew angle 30°, $a/h = 10$, SSSS

Figure 7 Continued

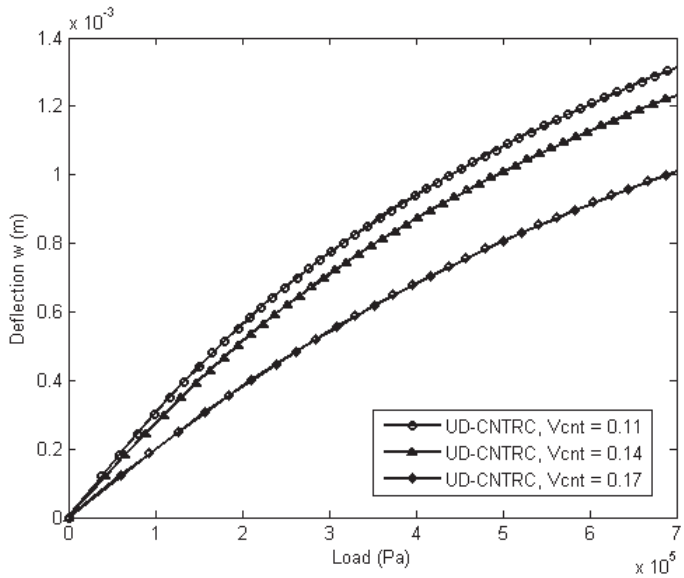

(b) Skew angle 30°, $a/h = 10$, type UD, SSSS

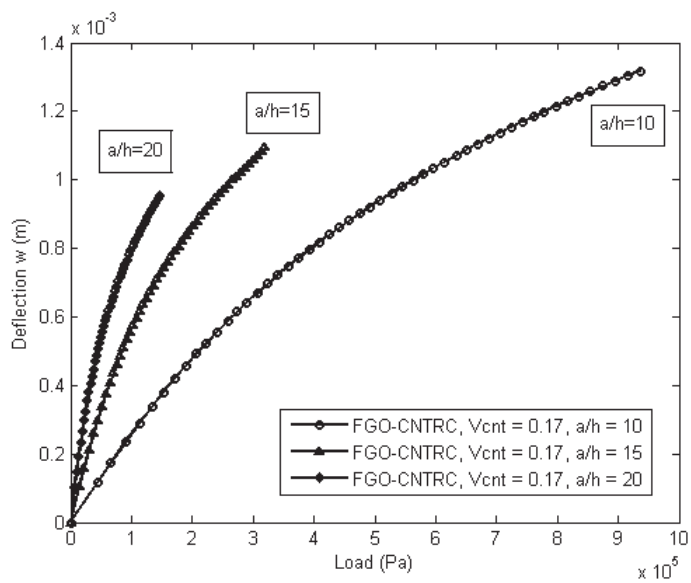

(c) Skew angle 30°, type FG-O, $a/b = 1$, SSSS

Figure 7 Continued

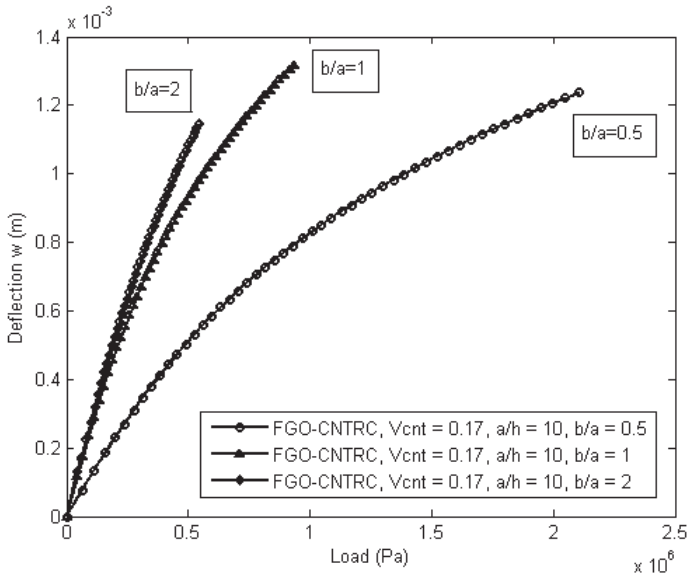

(d) Skew angle 30°, $a/h = 10$, type FG-O, SSSS

Figure 7 The deflection-load curves with several kind of properties.

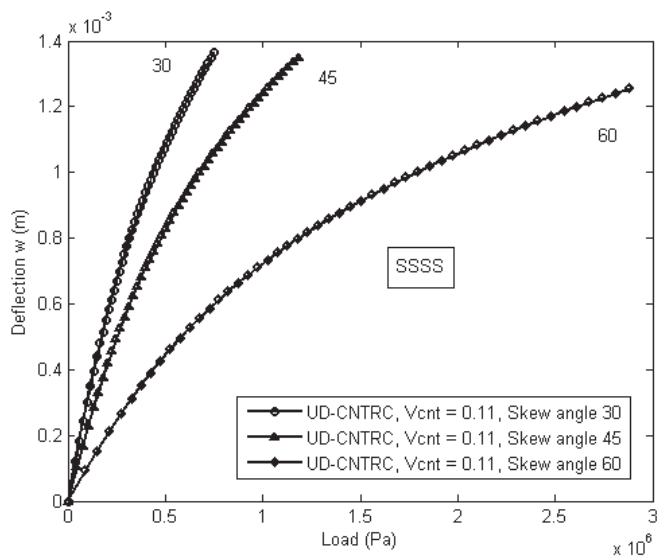

(a) $b/a = 1$, $a/h = 10$, type UD

Figure 8 Continued

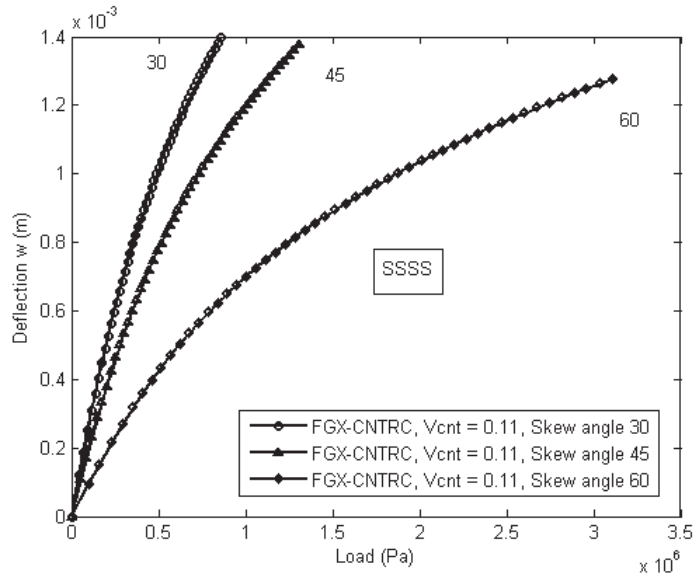

(b) $b/a = 1$, $a/h = 10$, type FG-X

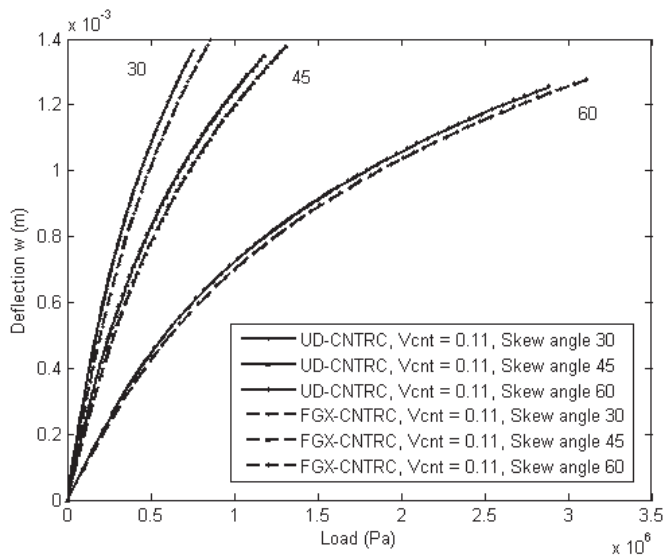

(c) Combination of two types UD and FG-X with (SSSS)

Figure 8 The effect of skew angle on the nonlinear bending behavior of (SSSS) FG-CNTRC skew plates.

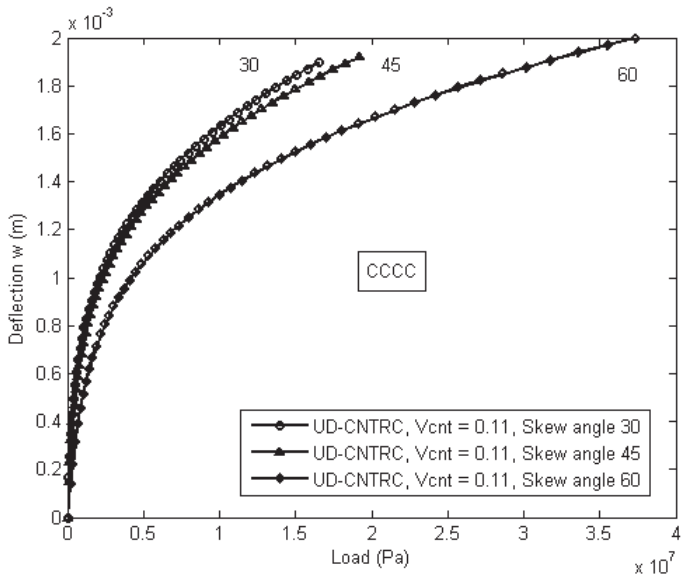

(a) $b/a = 1$, $a/h = 10$, type UD

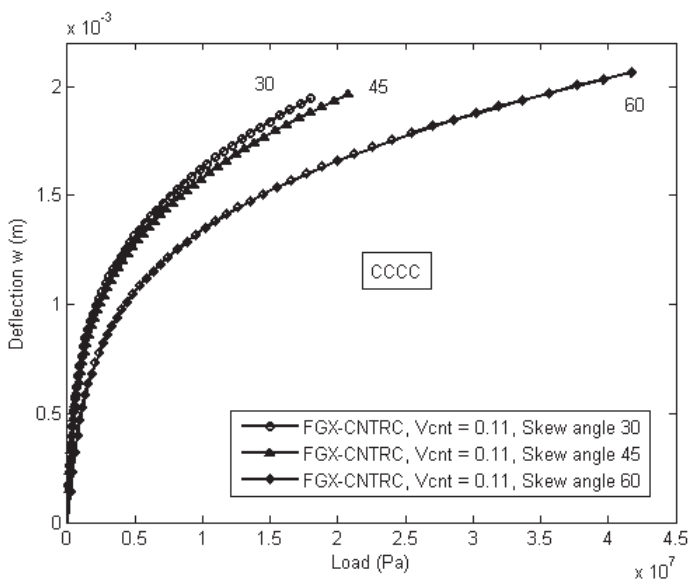

(b) $b/a = 1$, $a/h = 10$, type FG-X

Figure 9 Continued

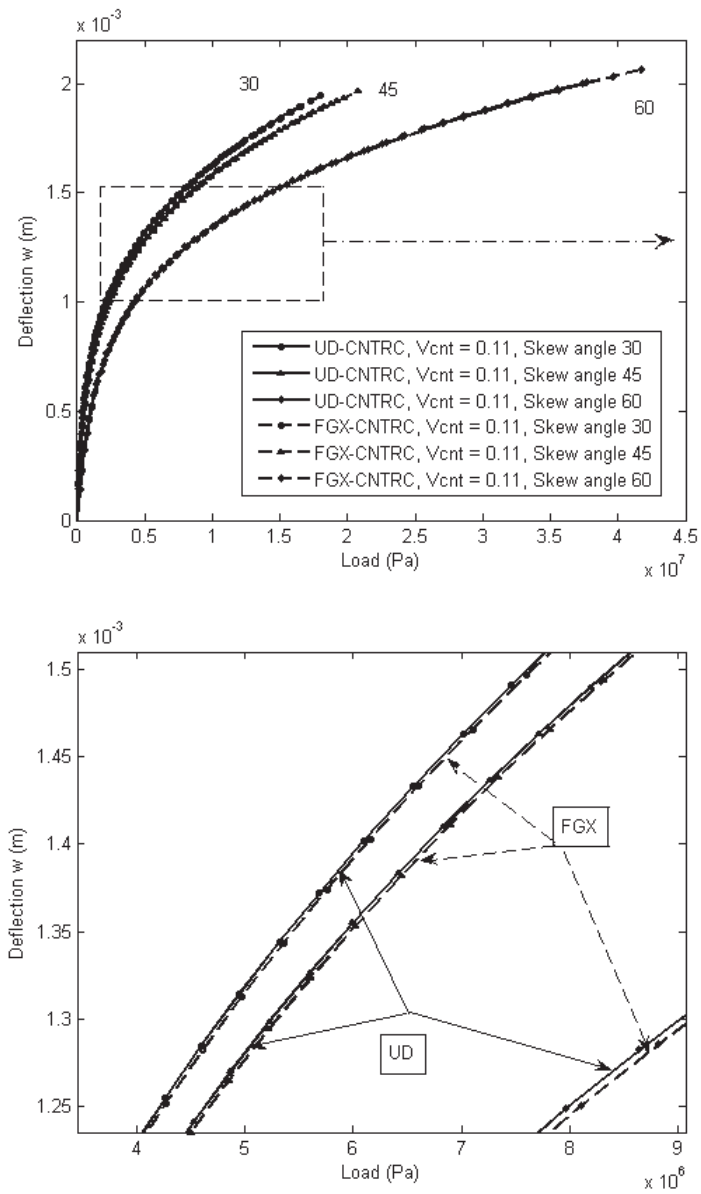

(c) Combination of two types UD and FG-X with (CCCC)

Figure 9 The effect of skew angle on the nonlinear bending behavior of (CCCC) FG-CNTRC skew plates.

Figures 9(a) and 9(b), but still complies with the previous comments as zoomed in Figure 9(c).

5 Conclusion

An efficient element based on the C^0-type of Shi's third-order shear deformation theory (C^0-STSDT) is employed to examine the linear and nonlinear behaviors of FG-CNTRC plates. The idea behind the present study is firstly introduced an alternative approach to the problems related to FG-CNTRC plate structures. Based on the C^0-type of Shi theory, all finite element matrices for linear as well as nonlinear analysis are established. Various numerical investigations are conducted to verify that the results of the proposed element are completely reliable with no regrettable phenomena.

References

[1] P. J. F. Harris, "Carbon Nanotubes and Related Structures: New Materials for the Twenty-First Century," *American Journal of Physics*, vol. 72, pp. 415–415, 2004.

[2] S. Iijima, "Helical microtubules of graphitic carbon," *Nature*, vol. 354, pp. 56–58, 1991.

[3] Y. Han and J. Elliott, "Molecular dynamics simulations of the elastic properties of polymer/carbon nanotube composites," *Computational Materials Science*, vol. 39, pp. 315–323, 2007.

[4] J. N. Coleman, U. Khan, W. J. Blau, and Y. K. Gun'ko, "Small but strong: A review of the mechanical properties of carbon nanotube–polymer composites," *Carbon*, vol. 44, pp. 1624–1652, 2006.

[5] M. M. Shokrieh and R. Rafiee, "A review of the mechanical properties of isolated carbon nanotubes and carbon nanotube composites," *Mechanics of Composite Materials*, vol. 46, pp. 155–172, 2010.

[6] A. K.-T. Lau and D. Hui, "The revolutionary creation of new advanced materials—carbon nanotube composites," *Composites Part B: Engineering*, vol. 33, pp. 263–277, 2002.

[7] E. Providas and M. A. Kattis, "An assessment of two fundamental flat triangular shell elements with drilling rotations," *Comput Struct*, vol. 77, pp. 129–139, 2000.

[8] C.-K. Choi and T.-Y. Lee, "Efficient remedy for membrane locking of 4-node flat shell elements by non-conforming modes," *Comput Method Appl M*, vol. 192, pp. 1961–1971, 2003.

[9] H. T. Y. Yang, S. Saigal, A. Masud, and R. K. Kapania, "A survey of recent shell finite elements," *Int J Numer Meth Eng*, vol. 47, pp. 101–127, 2000.

[10] A. W. Leissa, "A Review of Laminated Composite Plate Buckling," *Appl Mech Rev*, vol. 40, pp. 575–591, 1987.

[11] M. Aydogdu, "Comparison of Various Shear Deformation Theories for Bending, Buckling, and Vibration of Rectangular Symmetric Cross-ply Plate with Simply Supported Edges," *J Compos Mater*, vol. 40, pp. 2143–2155, 2006.

[12] K. M. Liew, K. C. Hung, and M. K. Lim, "Three-dimensional vibration of rectangular plates : Variance of simple support conditions and influence of in-plane inertia," *Int J Solids Struct*, vol. 31, pp. 3233–3247, 1994.

[13] K. M. Liew, K. C. Hung, and M. K. Lim, "Three-dimensional vibration of rectangular plates: Effects of thickness and edge constraints," *J Sound Vib*, vol. 182, pp. 709–727, 1995.

[14] P.-S. Lee and K.-J. Bathe, "The quadratic MITC plate and MITC shell elements in plate bending," *Adv Eng Softw*, vol. 41, pp. 712–728, 2010.

[15] C. H. Thai, A. J. M. Ferreira, S. P. A. Bordas, T. Rabczuk, and H. Nguyen-Xuan, "Isogeometric analysis of laminated composite and sandwich plates using a new inverse trigonometric shear deformation theory," *Eur J Mech A-Solid*, vol. 43, pp. 89–108, 2014.

[16] C. H. Thai, L. V. Tran, D. T. Tran, T. Nguyen-Thoi, and H. Nguyen-Xuan, "Analysis of laminated composite plates using higher-order shear deformation plate theory and node-based smoothed discrete shear gap method," *Appl Math Model*, vol. 36, pp. 5657–5677, 2012.

[17] C. Thai-Hoang, N. Nguyen-Thanh, H. Nguyen-Xuan, and T. Rabczuk, "An alternative alpha finite element method with discrete shear gap technique for analysis of laminated composite plates," *Appl Math Comput*, vol. 217, pp. 7324–7348, 2011.

[18] L. T. That-Hoang, H. Nguyen-Van, T. Chau-Dinh, and C. Huynh-Van, "Enhancement to four-node quadrilateral plate elements by using cell-based smoothed strains and higher-order shear deformation theory for nonlinear analysis of composite structures," *Journal of Sandwich Structures & Materials*, vol. 22, pp. 2302–2329, 2018.

[19] T. Q. Bui, T. V. Do, L. H. T. Ton, D. H. Doan, S. Tanaka, D. T. Pham, *et al.*, "On the high temperature mechanical behaviors analysis of heated functionally graded plates using FEM and a new third-order shear deformation plate theory," *Composites Part B: Engineering*, vol. 92, pp. 218–241, 2016.

[20] H. L. Ton-That, H. Nguyen-Van, and T. Chau-Dinh, "An Improved Four-Node Element for Analysis of Composite Plate/Shell Structures Based on Twice Interpolation Strategy," *International Journal of Computational Methods*, vol. 17, 1950020, 2019.

[21] H. L. Ton That, H. Nguyen-Van, and T. Chau-Dinh, "Nonlinear Bending Analysis of Functionally Graded Plates Using SQ4T Elements based on Twice Interpolation Strategy," *Journal of Applied and Computational Mechanics*, vol. 6, pp. 125–136, 2020.

[22] H. L. Ton-That, "Finite Element Analysis of Functionally Graded Skew Plates in Thermal Environment based on the New Third-order Shear Deformation Theory," *Journal of Applied and Computational Mechanics*, vol. 6, pp. 1044–1057, 2020.

[23] H. L. Ton-That, "Improvement on eight-node quadrilateral element (IQ8) using twice-interpolation strategy for linear elastic fracture mechanics," *Engineering Solid Mechanics*, vol. 8, pp. 323–336, 2020.

[24] S. Ahmad, B. M. Irons, and O. C. Zienkiewicz, "Analysis of thick and thin shell structures by curved finite elements," *International Journal for Numerical Methods in Engineering*, vol. 2, pp. 419–451, 1970.

[25] T. J. R. Hughes and E. Carnoy, "Nonlinear finite element shell formulation accounting for large membrane strains," *Computer Methods in Applied Mechanics and Engineering*, vol. 39, pp. 69–82, 1983.

[26] H. L. Ton That, "A Novel Quadrilateral Element for Dynamic Response of Plate ?Structures Subjected to Blast Loading," *Journal of Applied and Computational Mechanics*, 2020.

[27] J. Argyris and L. Tenek, "Linear and geometrically nonlinear bending of isotropic and multilayered composite plates by the natural mode method," *Computer Methods in Applied Mechanics and Engineering*, vol. 113, pp. 207–251, 1994.

[28] F. van Keulen, "A geometrically nonlinear curved shell element with constant stress resultants," *Computer Methods in Applied Mechanics and Engineering*, vol. 106, pp. 315–352, 1993.

[29] C. Sansour and H. Bednarczyk, "The Cosserat surface as a shell model, theory and finite-element formulation," *Computer Methods in Applied Mechanics and Engineering*, vol. 120, pp. 1–32, 1995.

[30] A. Kamoulakos, "Understanding and improving the reduced integration of Mindlin shell elements," *International Journal for Numerical Methods in Engineering*, vol. 26, pp. 2009–2029, 1988.

[31] W. K. Liu, Y.-K. Hu, and T. Belytschko, "Multiple quadrature underintegrated finite elements," *International Journal for Numerical Methods in Engineering*, vol. 37, pp. 3263–3289, 1994.

[32] X. Hu, T. Q. Bui, J. Wang, W. Yao, L. H. T. Ton, I. V. Singh, *et al.*, "A new cohesive crack tip symplectic analytical singular element involving plastic zone length for fatigue crack growth prediction under variable amplitude cyclic loading," *European Journal of Mechanics - A/Solids*, vol. 65, pp. 79–90, 2017.

[33] J. C. Simo and M. S. Rifai, "A class of mixed assumed strain methods and the method of incompatible modes," *International Journal for Numerical Methods in Engineering*, vol. 29, pp. 1595–1638, 1990.

[34] J. C. Simo, F. Armero, and R. L. Taylor, "Improved versions of assumed enhanced strain tri-linear elements for 3D finite deformation problems," *Computer Methods in Applied Mechanics and Engineering*, vol. 110, pp. 359–386, 1993.

[35] H. Parisch, "An investigation of a finite rotation four node assumed strain shell element," *International Journal for Numerical Methods in Engineering*, vol. 31, pp. 127–150, 1991.

[36] J. Jang and P. M. Pinsky, "Convergence of curved shell elements based on assumed covariant strain interpolations," *International Journal for Numerical Methods in Engineering*, vol. 26, pp. 329–347, 1988.

[37] H. L. Ton-That and H. Nguyen-Van, "A Combined Strain Element in Static, Frequency and Buckling Analyses of Laminated Composite Plates and Shells," *Periodica Polytechnica Civil Engineering*, 2020.

[38] T. Kant, S. Kumar, and U. P. Singh, "Shell dynamics with three-dimensional degenerate finite elements," *Computers & Structures*, vol. 50, pp. 135–146, 1994.

[39] F. Gruttmann and W. Wagner, "Coupling of two- and three-dimensional composite shell elements in linear and non-linear applications," *Computer Methods in Applied Mechanics and Engineering*, vol. 129, pp. 271–287, 1996.

[40] A. Ibrahimbegoviæ and F. Frey, "Stress resultant geometrically nonlinear shell theory with drilling rotations—Part II. Computational aspects," *Computer Methods in Applied Mechanics and Engineering*, vol. 118, pp. 285–308, 1994.

[41] H. Nguyen-Van, H. L. Ton-That, T. Chau-Dinh, and N. D. Dao, "Nonlinear Static Bending Analysis of Functionally Graded Plates Using MISQ24 Elements with Drilling Rotations," *International Conference on Advances in Computational Mechanics*, Singapore, pp. 461–475, 2018.

[42] H. L. Ton-That;, H. Nguyen-Van;, and T. Chau-Dinh, "Static and buckling analyses of stiffened plate/shell structures using the quadrilateral element SQ4C," *Comptes Rendus. Mécanique*, vol. 348, pp. 285–305, 2020.

[43] L. Jiang, M. W. Chernuka, and N. G. Pegg, "A co-rotational, updated Lagrangian formulation for geometrically nonlinear finite element analysis of shell structures," *Finite Elements in Analysis and Design*, vol. 18, pp. 129–140, 1994.

[44] G. F. Moita and M. A. Crisfield, "A finite element formulation for 3-D continua using the co-rotational technique," *International Journal for Numerical Methods in Engineering*, vol. 39, pp. 3775–3792, 1996.

[45] C. L. Liao and J. N. Reddy, "Continuum-based stiffened composite shell element for geometrically nonlinear analysis," *AIAA Journal*, vol. 27, pp. 95–101, 1989.

[46] W. C. Chao and J. N. Reddy, "Analysis of laminated composite shells using a degenerated 3-D element," *International Journal for Numerical Methods in Engineering*, vol. 20, pp. 1991–2007, 1984.

[47] G. Shi, "A new simple third-order shear deformation theory of plates," *International Journal of Solids and Structures*, vol. 44, pp. 4399–4417, 2007.

[48] S. Imani Yengejeh, S. A. Kazemi, and A. Öchsner, "Carbon nanotubes as reinforcement in composites: A review of the analytical, numerical and experimental approaches," *Computational Materials Science*, vol. 136, pp. 85–101, 2017.

[49] F. T. Fisher, R. D. Bradshaw, and L. C. Brinson, "Fiber waviness in nanotube-reinforced polymer composites—I: Modulus predictions using effective nanotube properties," *Composites Science and Technology*, vol. 63, pp. 1689–1703, 2003.

[50] H.-S. Shen, "Nonlinear bending of functionally graded carbon nanotube-reinforced composite plates in thermal environments," *Composite Structures*, vol. 91, pp. 9–19, 2009.

[51] S. Sharma, R. Chandra, P. Kumar, and N. Kumar, "Molecular dynamics simulation of polymer/carbon nanotube composites," *Acta Mechanica Solida Sinica*, vol. 28, pp. 409–419, 2015.

[52] P. Zhu, Z. X. Lei, and K. M. Liew, "Static and free vibration analyses of carbon nanotube-reinforced composite plates using finite element method with first order shear deformation plate theory," *Composite Structures*, vol. 94, pp. 1450–1460, 2012.

[53] T. Truong-Thi, T. Vo-Duy, V. Ho-Huu, and T. Nguyen-Thoi, "Static and Free Vibration Analyses of Functionally Graded Carbon Nanotube Reinforced Composite Plates using CS-DSG3," *International Journal of Computational Methods*, vol. 17, 1850133, 2020.

[54] P. Phung-Van, M. Abdel-Wahab, K. M. Liew, S. P. A. Bordas, and H. Nguyen-Xuan, "Isogeometric analysis of functionally graded carbon nanotube-reinforced composite plates using higher-order shear deformation theory," *Composite Structures*, vol. 123, pp. 137–149, 2015.

[55] A. Alibeigloo and A. Emtehani, "Static and free vibration analyses of carbon nanotube-reinforced composite plate using differential quadrature method," *Meccanica*, vol. 50, pp. 61–76, 2015.

Biography

Hoang Lan Ton-That, an assistant professor, is a lecturer at the Ho Chi Minh City University of Architecture, Vietnam since summer 2003. He is also a visiting lecturer for universities in the south of Vietnam. He has obtained scientific degree at the University of Liege, Belgium. His areas of expertise include computational mechanics, meshfree methods, fracture mechanics, static, dynamic and buckling analysis of plate/shell structures, and smart materials.